Arabian Journal of Chemistry (2020) **13**, 4111–4125

King Saud University

Arabian Journal of Chemistry

www.ksu.edu.sa
www.sciencedirect.com

ORIGINAL ARTICLE

Fabrication of zirconium(IV) cross-linked alginate/kaolin hybrid beads for nitrate and phosphate retention

Ilango Aswin Kumar, Natrayasamy Viswanathan *

Department of Chemistry, Anna University, University College of Engineering - Dindigul, Reddiyarchatram, Dindigul - 624 622, Tamilnadu, India

Received 17 March 2019; accepted 13 June 2019
Available online 21 June 2019

KEYWORDS

Alginate;
Kaolin;
Zr^{4+} ions;
Zr@AlgKN beads;
NO_3^- and PO_4^{3-} adsorption;
Reuse

Abstract The extreme nitrate (NO_3^-) species in drinking water leads to methemoglobinemia (blue baby syndrome) disease in new born toddlers whereas the excess phosphate (PO_4^{3-}) and NO_3^- contents lead to the eutrophication (algae growth) problem of water sources. Upto date, the environmental researchers have developing the suitable adsorbent materials for providing NO_3^- and PO_4^{3-} free water system. In present study, a low-cost alginate (Alg) assisted kaolin (KN) (AlgKN) composite beads were prepared and utilized for the removal of NO_3^- and PO_4^{3-}. To improve the sorption capacity (SC) and stability, Zr^{4+} ions were coated onto AlgKN to get Zr@AlgKN composite beads which were prepared via., hydrothermal (Hydro) and in situ precipitation (In situ) methods. The hydro assisted Zr@AlgKN composite beads possess an enhanced SC than the in situ assisted adsorbents. In batch scale, the parameters responsible for the adsorption process such as contact time, co-ions, adsorbent dosage, pH, initial ions concentration and temperature were optimized. The adsorbents were characterized by XRD, FTIR, BET, EDAX and SEM analysis. The adsorption experimental data was fitted with isotherms, kinetics and thermodynamic parameters. The regeneration and field applicability study of the Zr@AlgKN composite beads were also investigated.

1. Introduction

Nitrogen (N) and phosphorus (P) are the essential macronutrients for all the existing organisms (Aswin Kumar and Viswanathan, 2018a). But, the extreme nitrate (NO_3^-) species in drinking water leads to methemoglobinemia (blue baby syndrome) in new born toddlers whereas the excess phosphate (PO_4^{3-}) and NO_3^- contents lead to the eutrophication (algae growth) problem of water sources (Fewtrell, 2004). The World Health Organization (WHO) has fixed the NO_3^- and PO_4^{3-} contents with 40 and <0.5 mg/L respectively are to be the tolerance limit in drinking water (Aswin Kumar and Viswanathan, 2018b). The rapid utilization of NO_3^- and PO_4^{3-} made vibration on

* Corresponding author.
E-mail address: drnviswanathan@gmail.com (N. Viswanathan).
Peer review under responsibility of King Saud University.

ELSEVIER Production and hosting by Elsevier

https://doi.org/10.1016/j.arabjc.2019.06.006
1878-5352

the environmental scientists to expand the modern techniques for removing them from water. The numerous NO_3^- and PO_4^{3-} removal technologies such as biological treatment (Meinhold et al., 1999), chemical precipitation (Guo et al., 2010), adsorption (Aswin Kumar and Viswanathan, 2018c), ion-exchange (Xing et al., 2010) and membrane process (Kyu-Hong et al., 2003) were investigated in which adsorption method seems to be cost-effective and suitable at industrial level.

Kaolin (KN) is a silicate type natural clay which containing the elemental constituents of aluminum oxide (Al_2O_3) (39.50%), silicon dioxide (SiO_2) (46.54%) and water (H_2O) molecule (13.96%) in its layered structure (Wang et al., 2009). The isomorphous replacement of Si^{4+} by Al^{3+} ions in the silicate double layer of KN clay makes it as the good adsorbent material for the contaminant adsorption from water (Adebowale et al., 2006). However, the bottle-necks of KN clay such as pressure drop during filtration and low-cation exchange capacity makes it as the unsuitable material for the practical use. To resolve this shortcut, biopolymeric composite beads have been investigated in recent years (Aswin Kumar and Viswanathan, 2017a).

Alginate (Alg) is a natural polysaccharide derived from the brown seaweeds. It has the monomers of (1/4) a-L-guluronate and (1/4) b-D-mannuronate in a unit (Pandi and Viswanathan, 2014). Alg has advantages like biodegradable, biocompatible and eco-friendly which make it as the prominent adsorbent material. In addition, the chemical modification of Alg increases its stability and reactivity toward the toxic ions adsorption. Hence, alginate supported kaolin (AlgKN) composite beads were prepared by dispersing KN clay in Alg matrix. In addition, Alg has the tendency to interact with higher valence metal ions to form metal-alginate complex beads (Pandi and Viswanathan, 2015).

Zirconium (IV) (Zr^{4+}) is an inorganic metal ion belonging to d-block family. Zr^{4+} ion fit in to Lewis acid category which easily binds the Lewis bases like NO_3^- and PO_4^{3-}. Hence, Zr^{4+} ions were uniformly cross-linked with AlgKN composite beads to form Zr^{4+} loaded AlgKN (Zr@AlgKN) composite beads. The adsorbent preparation by hydrothermal method using an autoclave has enriches the material properties via, smaller the particle size with larger the specific surface area which leads to the higher sorption capacity (SC) of the adsorbent (Ahmed et al., 2017). Sorption capacity is defined as the amount of adsorbate (mg) adsorbed per unit gram of the adsorbent.

This present investigation was focused to synthesize in situ and hydro assisted Zr@AlgKN composite beads for the NO_3^- and PO_4^{3-} adsorption. The characterization studies such as XRD, FTIR, BET, EDAX and SEM analysis of the adsorbents were performed. The parameters responsible for adsorption process such as contact time, pH, dosage, initial ions concentration, temperature and co-ions were optimized in batch scale. The isotherms and study of thermodynamic parameters were carried out. The kinetic study of Zr@AlgKN composite beads (Hydro) were performed to find the order of NO_3^- and PO_4^{3-} adsorption. The field study and regeneration of the Zr@AlgKN composite beads were also investigated.

2. Experimental section

2.1. Materials

Sodium alginate (70,000–80,000 of molecular weight) was acquired from Himedia, India. $ZrOCl_2{\cdot}8H_2O$ (98.0%), Kaolin clay, NaOH (≥98.0%), HCl (35–38%), NH_4VO_3 (98.0%) and $(NH_4)_6Mo_7O_{24}$ (≥99.0%) was acquired from Merck, India. The typical PO_4^{3-} and NO_3^- stock solutions were prepared by dissolving of 1.4329 g of anhydrous KH_2PO_4 (≥98.0%) and 1.6305 g of anhydrous KNO_3 (≥98.0%) in 1000 mL of double distilled (DD) water separately. AR grade of all other reagents were utilized.

2.2. Synthesis of the composite beads

2.2.1. Preparation of alginate/kaolin (AlgKN) composite beads

About 2% of alginate solution was prepared by pouring 2 g of sodium alginate in 100 mL of DD water. About 10 g of Kaolin clay was dispersed in DD water which is slowly poured into alginate medium and continuously stirred using magnetic stirrer for 3 h to get homogeneous AlgKN composite solution. Then, AlgKN composite solution was taken in the burette and slowly dropped into 2% $CaCl_2$ to obtain AlgKN composite beads. Further, it was kept undisturbed in the same solution upto 24 h for ageing as well as strengthening of the beads. For hydro synthesis, the wet AlgKN composite beads were transmitted into Teflon shielded autoclave and heated to 130 °C for 6 h. Finally, AlgKN composite beads were filtered by centrifuge and dried in hot air oven at 80 °C upto 4 h for NO_3^- and PO_4^{3-} adsorption studies.

2.2.2. Preparation of Zr^{4+} ions coated AlgKN (Zr@AlgKN) composite beads

To prepare Zr@AlgKN composite beads, about 3% of Zr^{4+} solution was prepared which is taken in the glass beaker (100 mL). Further, the prepared homogeneous AlgKN composite solution was taken in the burette and slowly dropped into Zr^{4+} medium. Immediately, the usable Zr@AlgKN composite beads were formed. The obtained in situ assisted Zr@AlgKN composite beads were kept undisturbed in the mother liquid upto 24 h for ageing and as well as strengthening purpose. For hydro synthesis, the wet Zr@AlgKN composite beads were transmitted into Teflon shielded autoclave and heated to 130 °C for 7 h. Finally, the Zr@AlgKN composite beads were filtered by centrifuge and dried in hot air oven at 80 °C upto 4 h for NO_3^- and PO_4^{3-} adsorption studies.

2.3. NO_3^- and PO_4^{3-} adsorption by batch method

The batch adsorption tests were executed for NO_3^- and PO_4^{3-} adsorption. About 0.1 g of the adsorbent was added with 50 mL of 100 mg/L of the NO_3^- and PO_4^{3-} solutions which were taken in the iodine flask. The reaction contents were shaken under mechanical shaker at assorted time interval of 10 to 60 min and then the adsorbents were filtered by centrifuge followed by the final concentration of NO_3^- and PO_4^{3-} ions was analyzed by UV–Visible spectrophotometer. For hydrothermal preparation of the adsorbent, Teflon shielded autoclave (100 mL) was utilized at 130 °C. The parameters responsible for the adsorption process such as contact time, adsorbent dosage, pH, co-ions and initial ions concentration were carried out. About 0.1 N HCl/ NaOH were used to adjust the pH of the NO_3^- and PO_4^{3-} solution. The adsorption isotherms and kinetics study were executed for 80, 100, 120 and 140 mg/L of NO_3^- and PO_4^{3-} solution at 303, 313 and 323 K. The regeneration of the prepared Zr@AlgKN composite beads was studied using the suitable eluent NaOH in batch mode. The SC of the adsorbent and the removal percentage toward NO_3^-/PO_4^{3-} can be calculated by the Eqs. (1) and (2) as follows

$$\text{Sorption capacity(SC)} = \frac{C_i - C_e}{m} V \text{ mg/g} \quad (1)$$

$$\text{Removal efficiency} = \frac{C_i - C_e}{C_i} 100\% \quad (2)$$

where C_i and C_e are the initial and final concentration (mg/L) of both NO_3^- and PO_4^{3-} at equilibrium time, m is the amount of adsorbent (g) and V is the volume of adsorbate (L).

2.4. Analysis and characterization details

The NO_3^- and PO_4^{3-} concentration was analyzed using UV–Visible spectrophotometer kit (model: Spectroquant Pharo 300, Merck) at 202 and 400 nm respectively. To check the PO_4^{3-} concentration, the reagents such as NH_4VO_3 and $(NH_4)_6Mo_7O_{24}$ were utilized. To identify the pH of NO_3^- and PO_4^{3-} solution, pH electrode with Thermo Orion Benchtop multiparameter kit (model: VERSA STAR92) was used. The pH drift method was applied to determine the pH at zero point charge (pH_{zpc}) of the adsorbent (Lopez-Ramon et al., 1999). The quality parameters of drinking water such as chloride, total dissolved solids and total hardness was also studied using the standard methods (APHA, 2005).

The crystalline nature of the adsorbent was studied using X-ray diffraction (XRD) analysis by X'pert 173 PRO model PAN-alytical instrument. The surface textural properties of the adsorbents were observed by BET surface analyzer (model: NOVA 1000) at N_2 atmosphere. The functional groups present in the adsorbents were examined by Fourier transform infrared (FTIR) spectrometer (model: JASCO-460 plus). The particle size and surface topography of the beads were observed by scanning electron microscope (SEM) (model: Vega3 Tescan). The elemental accumulation of the hydro supported Zr@AlgKN composite beads and NO_3^-/PO_4^{3-} sorbed Zr@AlgKN composite beads were studied using energy dispersive X-ray analyzer (EDAX) (model: Bruker Nano GMBH).

2.5. Statistical tools

All the experimental data was computed by Microcal Origin (version 15) software. In addition, the chi-square analysis (χ^2), standard deviation (sd) and regression correlation coefficient (r) was utilized to fit the appropriate isotherm model.

3. Results and discussion

3.1. Characterization studies

3.1.1. FTIR investigation

FTIR study was used to identify the functional groups of the sodium alginate, kaolin (KN) clay, hydro assisted $ZrO(OH)_2$, AlgKN composite beads, Zr@AlgKN composite beads, NO_3^- and PO_4^{3-} adsorbed Zr@AlgKN composite beads which are shown in Fig. 1a–c. In FTIR spectra of sodium alginate, the -OH stretching vibration was observed at 3443 cm^{-1} whereas the asymmetric and symmetric vibrations of —COO group were attained at 1614 and 1423 cm^{-1} respectively (Aswin Kumar and Viswanathan, 2017b) (cf. Fig. 1a). In FTIR spectra of KN clay, the —OH stretching bands were attained at 3677 and 3429 cm^{-1} which due to the grafting of —OH with Al site of KN clay (Njoya et al., 2006). Further, Si—O and Si—O—Si vibrations in KN clay were observed at 1608 and 1049 cm^{-1} respectively. In addition, the -OH bending vibration of Al—OH in KN clay was pertained at 963 cm^{-1} (Georges-Ivo, 2005) (cf. Fig. 1a).

In FTIR spectra of $ZrO(OH)_2$, the symmetric and asymmetric frequencies of Zr—O—H was observed at 1391 and 1278 cm^{-1}, while Zr—O and O—H bending modes was attained at 1030 cm^{-1}. Mainly, the vibration bands of Zr—OH and Zr—O—Zr of $ZrO(OH)_2$ were appeared at 645 and 480 cm^{-1} respectively (Mekhemer, 1998) (cf. Fig. 1a). The individual FTIR bands of sodium alginate, KN clay and $ZrO(OH)_2$ were retained in the FTIR spectra of Zr@AlgKN composite beads which shows its good formation (cf. Fig. 1b). In FTIR spectra of NO_3^- and PO_4^{3-} adsorbed Zr@AlgKN composite beads, most of the significant FTIR bands of Zr@AlgKN composite beads were retained and shifted in wave-numbers which may confirms the NO_3^- and PO_4^{3-} adsorption. In addition, the asymmetric stretching and bending modes of PO_4^{3-} at 1032 and 560 cm^{-1} in PO_4^{3-} sorbed Zr@AlgKN composite beads may confirms PO_4^{3-} adsorption in Zr@AlgKN composite beads (cf. Fig. 1c) (Niwas et al., 2000).

3.1.2. XRD study

XRD spectra of sodium alginate, KN clay, hydro assisted Zr@AlgKN composite beads are shown in Fig. 1d. The two typical crystalline peaks of sodium alginate was appeared at 14.30° and 21.30° on the crystal planes (4 2 2) and (5 1 1) respectively (Zhao et al., 2015). In KN clay, the XRD signals at 12.30°, 21.92°, 23.98°, 34.02°, 36.80°, 42.98° and 61.95° was observed on the planes (0 0 1), (1 1 1), (0 2 1), (1 0 2), (2 0 0), (0 4 1) and (0 0 2) respectively [JCPDS File No. 78-2110] (Fardjaoui et al., 2017). Moreover, the XRD peaks of $ZrO(OH)_2$ are preserved at 30.01°, 35.55°, 50.09° and 61.02° in the crystalline planes (1 0 0), (1 0 2), (1 3 0) and (1 2 0) (Cui et al., 2012). It was concluded that the strong and individual XRD peaks of sodium alginate, KN clay and $ZrO(OH)_2$ were retained in the XRD spectra of Zr@AlgKN composite beads (Hydro) with crystalline nature which enhances the structural stability of the Zr@AlgKN composite beads (Hydro).

3.1.3. BET study

The textural properties of the in situ and hydro assisted Zr@AlgKN composite beads were studied using BET analysis. The N_2 adsorption/desorption isotherm graph of Zr@AlgKN composite beads (Hydro) were studied at 77 K and the pore size distribution of Zr@AlgKN composite beads (Hydro) were demonstrated in Fig. 2a and b respectively. The non-local density functional theory (NLDFT) method was applied to find the BET property of the beads. The specific surface area, total pore width and as well as pore volume of the hydro assisted Zr@AlgKN composite beads were found to be 78.93 m^2/g, 3.61 nm and 0.024 cm^3/g whereas for in situ assisted Zr@AlgKN composite beads it was found to be 67.15 m^2/g, 3.02 nm and 0.018 cm^3/g respectively. From BET results, it was observed that the hydro supported Zr@AlgKN composite beads possess the higher specific surface area, larger pore width and as well as pore volume compared to the in situ supported Zr@AlgKN composite beads. Hence, the NO_3^- and PO_4^{3-} ions can easily occupies the active sites of the hydro supported Zr@AlgKN composite beads than the in situ assisted Zr@AlgKN composite beads.

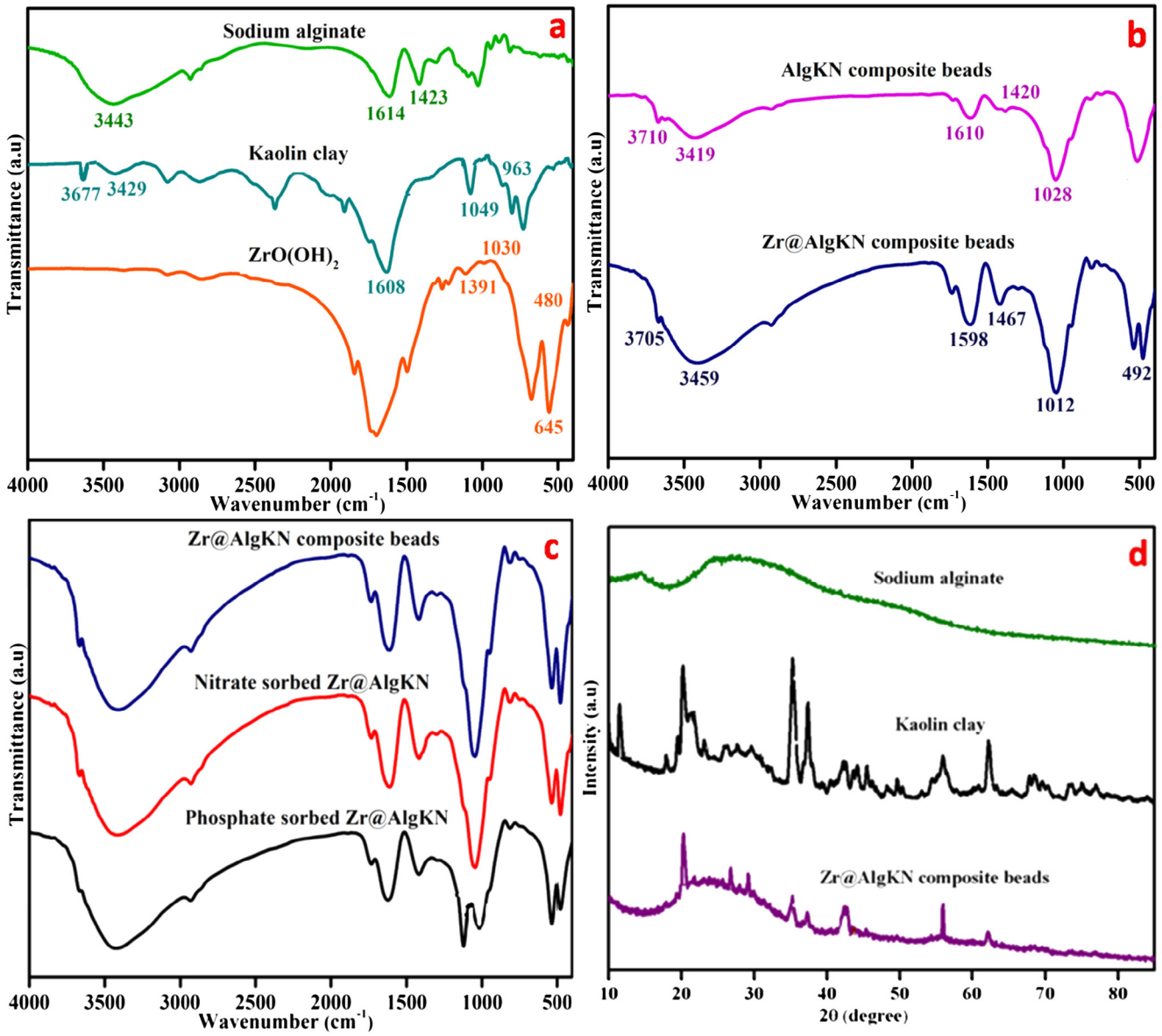

Fig. 1 FTIR spectra of (a) sodium alginate, kaolin clay and hydro assisted $ZrO(OH)_2$, (b) AlgKN and Zr@AlgKN composite beads, (c) Zr@AlgKN composite beads, nitrate sorbed Zr@AlgKN and phosphate sorbed Zr@AlgKN composite beads, and (d) XRD images of sodium alginate, kaolin clay and hydro assisted Zr@AlgKN composite beads.

3.1.4. SEM analysis

The surface morphology of in situ and hydro supported Zr@AlgKN composite beads with their NO_3^-/PO_4^{3-} sorption were studied by SEM analysis which are illustrated in Fig. 3b to i. The digital image of Zr@AlgKN composite beads were shown in Fig. 3a. The particle size of in situ and hydro assisted Zr@AlgKN composite beads were measured using SEM which found to be 1.597 and 1.362 mm respectively (cf. Fig. 3b and f). The close view of the in situ assisted Zr@AlgKN composite beads surface were taken at 10 µm which shows the irregular surface (cf. Fig. 3c) whereas hydro assisted Zr@AlgKN composite beads possess the uneven and needle like surface with some pores which is presented in Fig. 3g. The uneven surface of in situ assisted Zr@AlgKN composite beads was changed into smoother after NO_3^- and PO_4^{3-} adsorption (cf. Fig. 3d and e). Likewise, the active surface of hydro assisted Zr@AlgKN composite beads were almost blocked by NO_3^- and PO_4^{3-} ions result in the smoother surface which confirms the NO_3^- and PO_4^{3-} adsorption (cf. Fig. 3h and i).

3.1.5. EDAX analysis

The elemental components of hydro assisted Zr@AlgKN composite beads with their NO_3^- and PO_4^{3-} sorption were studied by EDAX analysis. In Fig. 4a, the significant elements of Zr@AlgKN composite beads such as O and C peaks from alginate, Si and Al peaks from kaolin clay and Zr peak were observed. Fig. 4b of NO_3^- sorbed Zr@AlgKN composite beads, in addition to C, O, Si, Al and Zr, the N (2.96%) peak were appeared with good percentage which may confirms NO_3^-

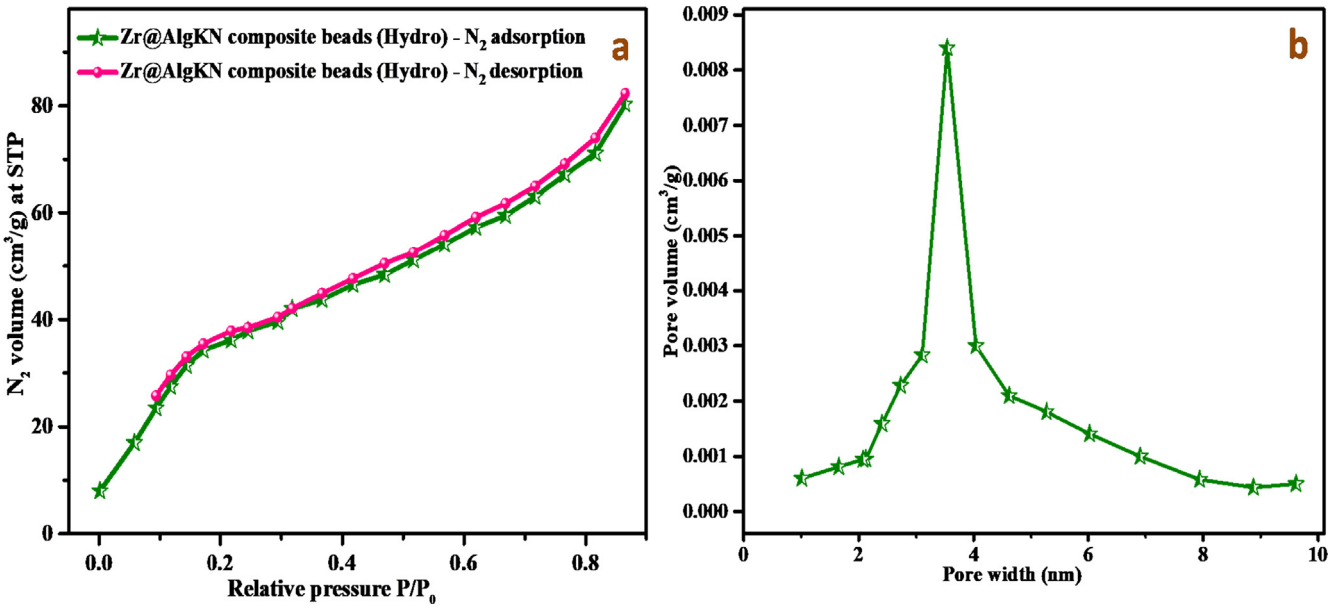

Fig. 2 (a) N_2 adsorption/desorption isotherm of Zr@AlgKN composite beads (Hydro) at 77 K, and (b) pore size distribution of Zr@AlgKN composite beads (Hydro).

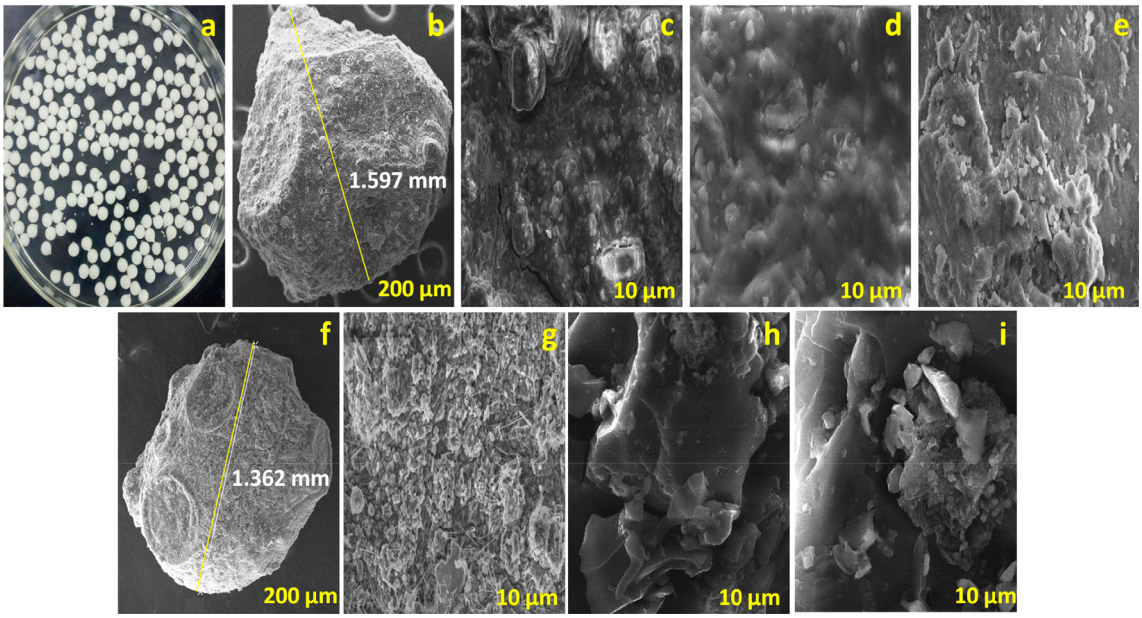

Fig. 3 (a) Digital image of Zr@AlgKN composite beads, SEM images of (b) particle size measured Zr@AlgKN composite beads (In situ) at 200 µm, (c) Zr@AlgKN composite beads (In situ) at 10 µm, (d and e) NO_3^- and PO_4^{3-} sorbed Zr@AlgKN composite beads (In situ), (f) particle size measured Zr@AlgKN composite beads (Hydro) at 200 µm, (g) Zr@AlgKN composite beads (Hydro) at 10 µm, and (h and i) NO_3^- and PO_4^{3-} sorbed Zr@AlgKN composite beads (Hydro).

sorption on Zr@AlgKN composite beads. In the case of PO_4^{3-} sorbed Zr@AlgKN, the new peak of P (3.37%) was appeared due to PO_4^{3-} adsorption (cf. Fig. 4c). It was also observed that from Fig. 4b and c, the atomic percentages of O, Si, Al and Zr was slightly low compared to the same in Fig. 4a may due to their interaction with NO_3^- and PO_4^{3-} during the adsorption process.

3.2. Effect of contact time

The contact time experiment was performed by adding 0.1 g of the adsorbent in 50 mL of 100 mg/L of the respective NO_3^- and PO_4^{3-} solution followed by stirred under mechanical shaker by assorted time interval of 10–60 min. The direct use of alginate

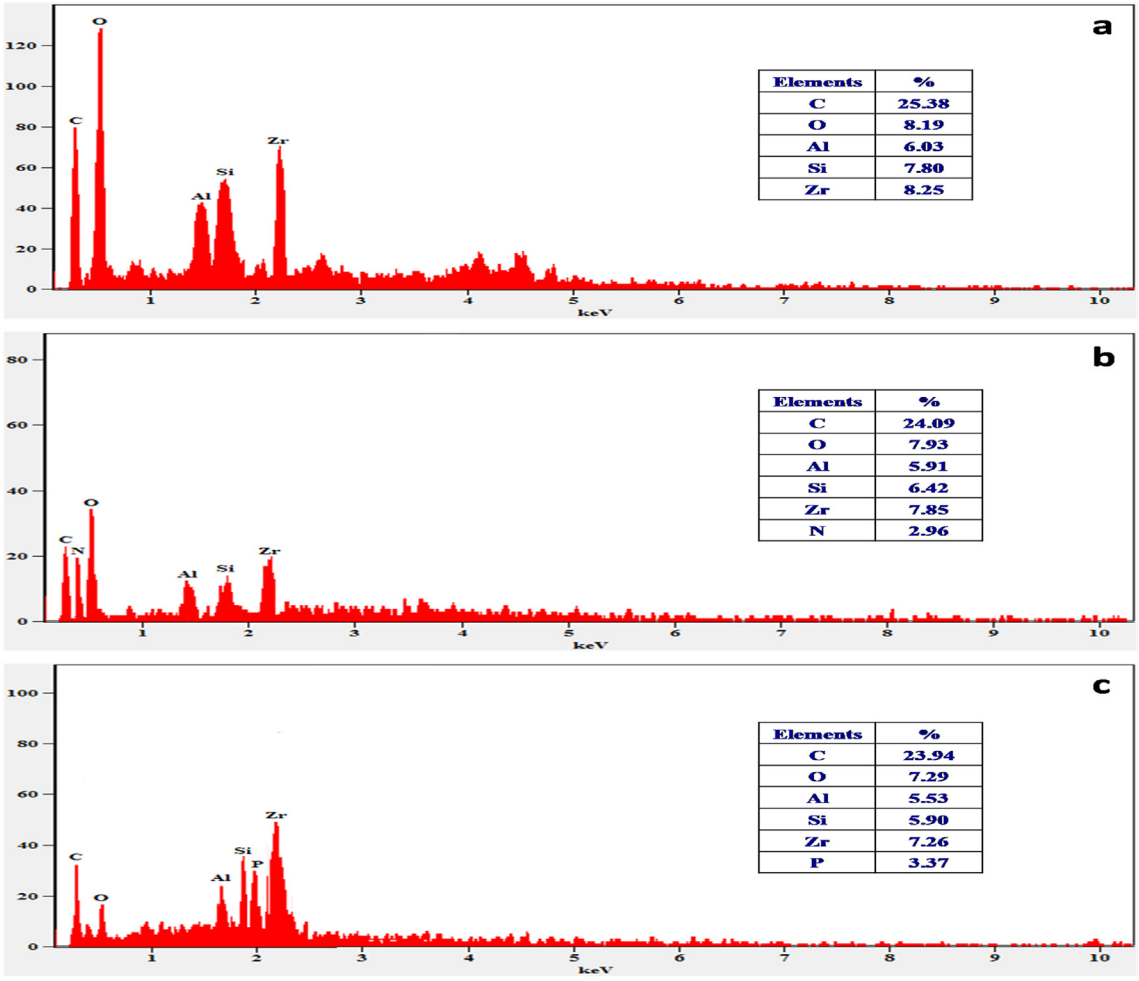

Fig. 4 EDAX spectra of hydro supported (a) Zr@AlgKN composite beads; (b) nitrate sorbed Zr@AlgKN composite beads, and (c) phosphate sorbed Zr@AlgKN composite beads.

(Alg) doesn't suits for the adsorption process due to its water soluble nature. Hence, the SCs of calcium alginate, KN clay, $ZrO(OH)_2$ (In situ), $ZrO(OH)_2$ (Hydro), AlgKN composite beads (In situ), AlgKN composite beads (Hydro), Zr@AlgKN beads (In situ) and Zr@AlgKN composite beads (Hydro) toward NO_3^- and PO_4^{3-} adsorption was shown in Fig. 5a and b respectively. It was found that Zr@AlgKN composite beads (Hydro) exhibit an enhanced SC of 31.24 and 37.18 mg/g toward NO_3^- and PO_4^{3-} with the equilibrium time of 30 min and other adsorbents were saturated at 40 min. In addition, Zr@AlgKN composite beads (In situ) possess the considerable SC. Hence, the further NO_3^- and PO_4^{3-} adsorption studies were investigated for both in situ and hydro assisted Zr@AlgKN composite beads with fixed contact time of 40 and 30 min respectively.

3.3. Effect of adsorbent dosage

The dosage effect of in situ and hydro assisted Zr@AlgKN composite beads toward NO_3^- and PO_4^{3-} adsorption were studied by taking the different dosages of Zr@AlgKN composite beads from 0.025 to 0.150 g. The correlation between SC and removal efficiency of the Zr@AlgKN composite beads toward NO_3^-/PO_4^{3-} adsorption with respect to varying the adsorbent dosage are shown in Fig. 5c and d respectively. The result portrays that raise of Zr@AlgKN composite beads dosage leads to increases the SC at initial and decreases after 0.1 g, whereas the removal percentage (%) was gradually increases because it does not depend on the amount of dosage. The active sites of the adsorbent would be more when the adsorbent dosage is high which results in the gradual increase in the removal efficiency toward the NO_3^-/PO_4^{3-} and lower in the SC after 0.1 g of the adsorbent dosage added. This is due to when the dosage of Zr@AlgKN composite beads increased, the availability in active sites is greater than the initial concentration of the NO_3^-/PO_4^{3-} thereby SC decreases after 0.1 g. (Farzana and Meenakshi, 2015). Hence, 0.1 g of the Zr@AlgKN composite beads was chosen as the optimum dosage.

3.4. Influence of initial ions concentration

The effect of initial concentrations of NO_3^- and PO_4^{3-} solution on its removal was studied. The varied initial concentrations such as 20, 40, 60, 80, 100, 120 and 140 mg/L of the NO_3^- and PO_4^{3-} solution was taken and added with 0.1 g of Zr@AlgKN composite beads. The results in Fig. 6a portrays

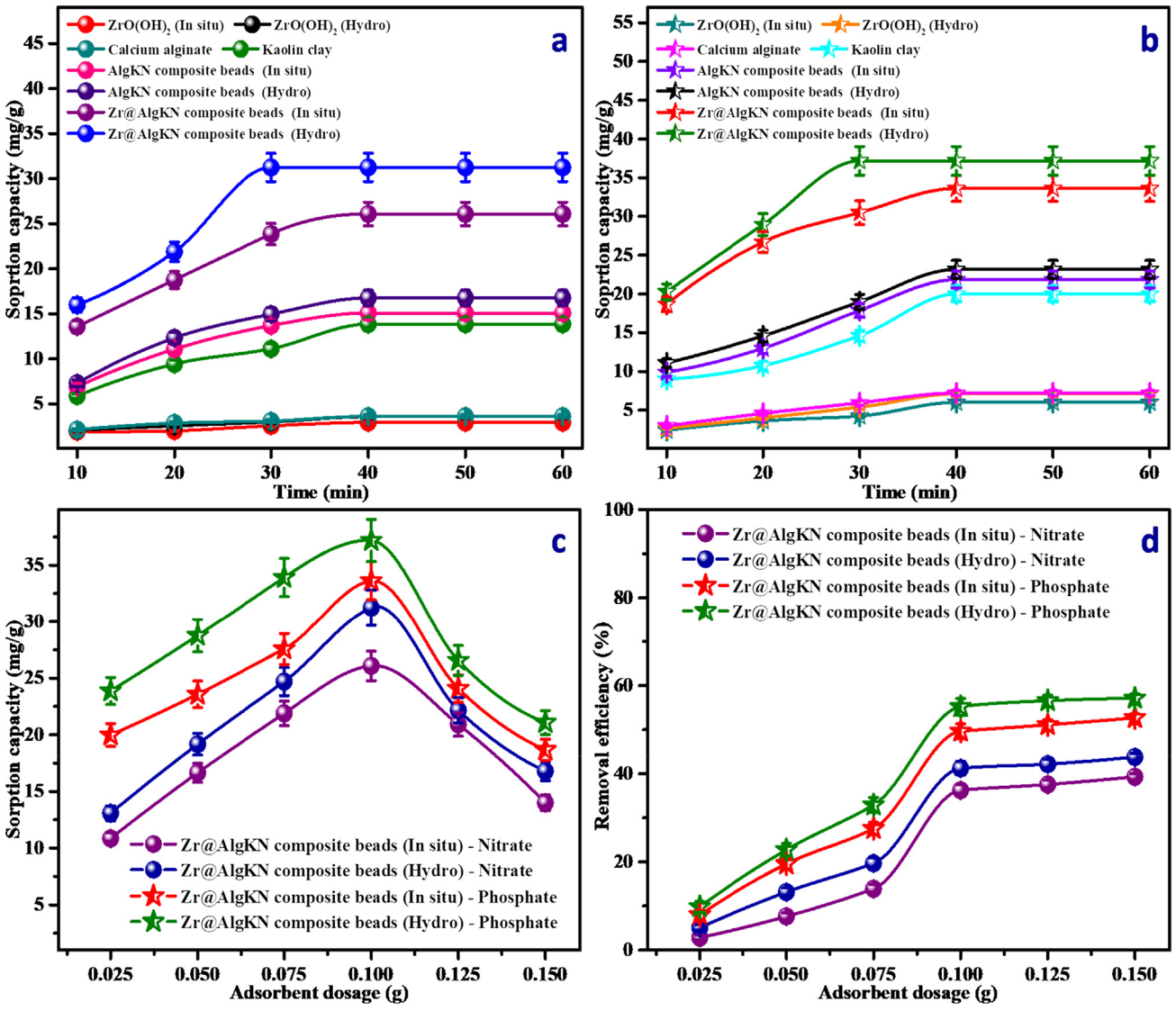

Fig. 5 Effect of (a and b) contact time of $ZrO(OH)_2$ (In situ), $ZrO(OH)_2$ (Hydro), calcium alginate, KN clay, AlgKN composite beads (In situ), AlgKN composite beads (Hydro), Zr@AlgKN composite beads (In situ) and Zr@AlgKN composite beads (Hydro) on the nitrate and phosphate SC respectively with 0.1 g of dosage at 10 to 60 min. Effect of (c and d) adsorbent dosage of in situ and hydro supported Zr@AlgKN composite beads on the nitrate and phosphate SC and removal efficiency respectively.

that SC toward NO_3^- and PO_4^{3-} was gradually increased with the raise of initial ions concentration followed by saturation was attained. The higher concentration of NO_3^-/PO_4^{3-} ions offer the mobile force which surmounts the mass transfer resistant at adsorbent/adsorbate surface thereby SC was increased (Karimi et al., 2012). Moreover, it was observed that the active sites of Zr@AlgKN composite beads were almost filled by NO_3^- and PO_4^{3-} ions at 100 mg/L. Hence, 100 mg/L of initial NO_3^-/PO_4^{3-} concentration was chosen as optimal concentration.

3.5. Influence of adsorbate pH

The solution pH is an important parameter which often affects the surface charge of the adsorbent. The effect of pH of NO_3^- and PO_4^{3-} solution on its adsorption was shown in Fig. 6b. In the case of NO_3^-, increasing pH from 3 to 5, SC was gradually increased and after pH 7 it was decreased. In the case of PO_4^{3-}, there was a gradual increase in SC which attained from pH 3 to 7 followed by decreased after pH 7. The several form of phosphate in water are H_3PO_4 (pH < 2), $H_2PO_4^-$ (pH 2 ~ 7), HPO_4^{2-} (pH 7 ~ 11) and PO_4^{3-} (pH > 11) respectively (Aswin Kumar and Viswanathan, 2018d). Amongst, $H_2PO_4^-$ (pH 2 ~ 7) is stable at acidic pH condition which leads to the increased phosphate SC upto pH 7. The pH_{zpc} values of the in situ and hydro supported Zr@AlgKN composite beads were found to be 5.31 and 5.64 respectively. From this values, it was concluded that the surfaces chare of Zr@AlgKN composite beads were positive and negative when the pH < pH_{zpc} and pH > pH_{zpc} respectively. Hence, during pH < pH_{zpc}, NO_3^- and PO_4^{3-} ions were surrounded with the protonated Zr@AlgKN composite beads by electrostatic attraction. However, in the basic pH condition, the predominant OH^- ions competes the NO_3^- and PO_4^{3-} adsorption by occupying the

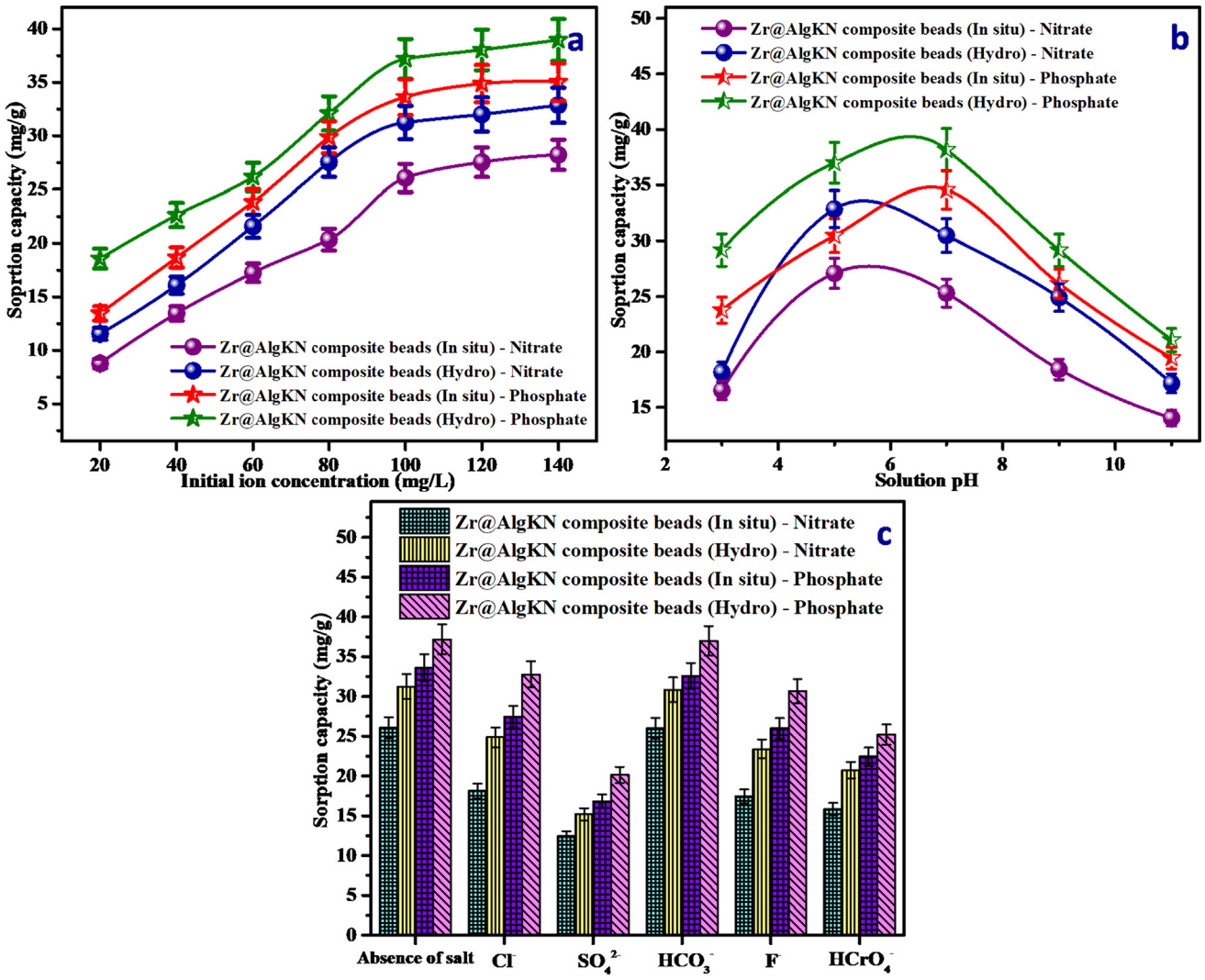

Fig. 6 Effect of (a) initial ions concentration, (b) pH of the solution, and (c) co-ions of the in situ and hydro assisted Zr@AlgKN composite beads on the nitrate and phosphate SC.

active sites of Zr@AlgKN composite beads during pH > pH_{zpc}. It was also observed that the pH of NO_3^- and PO_4^{3-} solution attaining neutral after the adsorption process which denotes the suitability of Zr@AlgKN composite beads at assorted pH conditions.

3.6. Influence of co-anions

In addition to NO_3^- and PO_4^{3-}, the other anions such as Cl^-, HCO_3^-, SO_4^{2-}, F^- and $HCrO_4^-$ are also present in the natural water which may affects the NO_3^- and PO_4^{3-} adsorption. About 0.1 g of Zr@AlgKN composite beads were added into 50 mL mixture containing 200 mg/L of the individual co-ion solution and 100 mg/L of NO_3^-/PO_4^{3-} solution. From Fig. 6c, it was observed that HCO_3^- ion does not compete significantly whereas the electronegative F^- and Cl^- ions slightly give the competition on the NO_3^-/PO_4^{3-} adsorption. The maximum SC toward NO_3^-/PO_4^{3-} adsorption was observed at acidic pH condition which was explained in the Section 3.5. However, $HCrO_4^-$ ions are also stable at acidic pH condition and hence it contends the NO_3^-/PO_4^{3-} adsorption. Moreover, SO_4^{2-} ion exhibit the predominant competing effect on the both NO_3^-/PO_4^{3-} adsorption due to its higher electronic charge and reactivity which make it as a competitor for NO_3^- and PO_4^{3-} by filling the active sites of the Zr@AlgKN composite beads instead of NO_3^-/PO_4^{3-} (Saad et al., 2007). The competing order of co-anions on NO_3^- and PO_4^{3-} adsorption was found to be $SO_4^{2-} > HCrO_4^- > F^- > Cl^- > HCO_3^-$.

3.7. Adsorption isotherms study

The isotherm study was performed to find the mechanism involved during NO_3^- and PO_4^{3-} adsorption by Zr@AlgKN composite beads. The experimental data was fitted with Freundlich (1906), Langmuir (1916) and Dubinin-Radushkevich (D-R) (Dubinin et al., 1947) isotherm models. About 0.1 g of Zr@AlgKN composite beads (Hydro) were added into 50 mL of individual NO_3^- and PO_4^{3-} solution having initial concentrations of 80, 100, 120 and 140 mg/L at 303, 313 and 323 K. The isotherm equations and their linear plot

details are shown in Table 1a. The single layer type of adsorption was governed by Langmuir which was plotted by C_e vs C_e/q_e. The multilayer type adsorption was governed by Freundlich which was plotted by log q_e vs log C_e and the best fit in these parameters are listed in Table 1b (Pahlavanzadeh et al., 2012). The 1/n and n values should be around 0 to 1 and 1 to 10 for the adsorption to be feasible. In Freundlich isotherm, it was detected that 1/n values dropping between 0 and 1 whereas n values falling between 1 and 10 denotes the favorable nature of NO_3^- and PO_4^{3-} adsorption onto Zr@AlgKN composite beads (Hydro).

The significant parameters such as K_{DR}, X_m, E, χ^2 and r of D-R isotherm was acquired by the plot of ln q_e vs ε^2 which are shown in Table 1b. The mean adsorption energy (E) value of Zr@AlgKN composite beads were found to be in the range of 7 to 10 kJ/mol which denotes the physisorption nature of NO_3^- and PO_4^{3-} adsorption (Wu, 2007). Mainly, the values of significant parameters such as χ^2, r and sd were used to determine the suitable isotherm model for NO_3^- and PO_4^{3-} adsorption. Langmuir isotherm exhibited the highest r value and lowest sd as well as χ^2 values toward NO_3^- adsorption whereas the same condition was applied for PO_4^{3-} adsorption by Freundlich isotherm which designates their respective suitability. The experimentally measured raw isotherm (c vs q) data was given in the supplementary file as Figs. S1 and S2, where the experimental data was compared with various isotherms.

3.8. Study of adsorption thermodynamics

The NO_3^- and PO_4^{3-} adsorption onto Zr@AlgKN composite beads (Hydro) were investigated through various thermodynamic parameters such as standard entropy change (ΔS°), Gibbs free energy change (ΔG°) and standard enthalpy change (ΔH°). The equations which were used to find out the thermodynamic parameters and their plot details are shown in Table 2a. From Table 2b, it was noticed that the decrease of Gibbs free energy change (ΔG°) with an increase of the temperature suggested the feasible adsorption process (Aswin Kumar and Viswanathan, 2018a). The negative enthalpy change (ΔH°) (−0.59 kJ/mol) points the exothermic nature of NO_3^- adsorption while the positive ΔH° (4.67 kJ/mol) spots the endothermic nature of PO_4^{3-} adsorption (Bhatnagar and Sillanpaa, 2011; Thagira Banu et al., 2018). The positive entropy change (ΔS°) value exposes the improved randomness in the liquid-solid interface in the surface of Zr@AlgKN

Table 1a Isotherm equations and their linear plot details.

Isotherms	Linear form	Linear plot	Parameters
Freundlich	$\log q_e = \log k_F + \frac{1}{n}\log C_e$	log q_e vs log C_e	q_e - Amount of NO_3^- and PO_4^{3-} adsorbed per unit weight of the sorbent (mg/g) C_e - Equilibrium concentration of NO_3^- and PO_4^{3-} solution (mg/L) k_F - Measure of sorption capacity 1/n - Adsorption intensity
Langmuir	$\frac{C_e}{q_e} = \frac{1}{Q^o b} + \frac{C_e}{Q^o}$	C_e/q_e vs C_e	Q^o - Amount of NO_3^- and PO_4^{3-} at complete monolayer coverage (mg/g) b - Langmuir isotherm constant (L/mg)
D-R	$\ln q_e = \ln X_m - k_{DR}\varepsilon^2$	ln q_e vs ε^2	X_m - NO_3^- and PO_4^{3-} adsorption capacity (mg/g) k - D-R isotherm constant ε^2 - Polanyi potential

Table 1b Isotherms of hydro supported Zr@AlgKN composite for NO_3^- and PO_4^{3-} adsorption.

Isotherms	Parameters	Nitrate			Phosphate		
		303 K	313 K	323 K	303 K	313 K	323 K
Freundlich	1/n	0.824	0.825	0.827	0.597	0.601	0.604
	n	6.315	6.317	6.319	7.051	7.055	7.058
	$k_F^{1/n}$ (mg/g) (L/mg)	28.135	28.129	28.120	32.816	32.827	32.831
	r	0.908	0.910	0.911	0.997	0.998	0.999
	sd	1.985	1.984	1.987	0.754	0.761	0.763
	χ^2	0.197	0.205	0.211	0.038	0.041	0.045
Langmuir	Q^o(mg/g)	31.241	31.218	31.189	37.182	37.201	37.230
	b (L/g)	0.931	0.938	0.944	1.065	1.068	1.067
	R_L	3.731	3.734	3.735	6.261	6.270	6.273
	r	0.992	0.990	0.993	0.986	0.987	0.989
	sd	0.567	0.582	0.634	2.764	2.767	2.769
	χ^2	0.017	0.019	0.021	0.437	0.442	0.446
Dubinin - Radushkevich	k_{DR} (mol^2/J^2)	4.86E-01	4.91E-01	4.95E-01	7.63E-01	7.68E-01	7.72E-01
	X_m (mg/g)	25.086	25.082	25.079	30.015	30.020	30.024
	E (kJ/mol)	8.097	8.122	8.123	9.164	9.169	9.701
	r	0.834	0.835	0.837	0.794	0.796	0.797
	sd	1.376	1.379	1.402	1.989	1.993	1.996
	χ^2	0.687	0.691	0.693	2.324	2.329	2.331

Table 2a Thermodynamic parameters, equations and linear plots.

Thermodynamic parameters	Thermodynamic equation	Thermodynamic linear plot	Parameters
Standard free energy change ΔG° (kJ/mol)	$\Delta G^\circ = -RT \ln K_o$	ln (q_e/C_e) vs C_e	T – Temperature
Standard enthalpy change ΔH° (kJ/mol)	$\ln K_o = \frac{\Delta S^\circ}{R} - \frac{\Delta H^\circ}{RT}$	ln K_o vs 1/T	R - Universal gas constant (8.314 J/mol K)
Standard entropy change ΔS° (J/K mol)	$S = (1 - \theta) \exp - [E_a/RT]$	ln (1 − θ) vs 1/T	K_o – Adsorption distribution coefficient

Table 2b Thermodynamic parameters of Zr@AlgKN composite beads.

Thermodynamic parameters		Nitrate	Phosphate
ΔG° (kJ/mol)	303 K	−3.16	−7.28
	313 K	−3.21	−7.35
	323 K	−3.29	−7.41
ΔH° (kJ/mol)		−0.59	4.67
ΔS° (J/K mol)		18.07	29.61

composite beads during NO_3^- and PO_4^{3-} adsorption (Bhatnagar et al., 2008; Aswin Kumar et al., 2019).

3.9. Kinetics study

To find the reaction rate of NO_3^- and PO_4^{3-} adsorption onto the hydro assisted Zr@AlgKN composite beads, the kinetic models such as reaction-based and diffusion-based models were investigated at 303, 313 and 323 K. The pseudo-first-order and pseudo-second-order kinetic models were categorized under the reaction based kinetic models. The kinetic equation and the linear plot details of these kinetic models are shown in Table 3a. The linear plot of pseudo-first-order was governed by log ($q_e - q_t$) vs t which shows its applicability whereas the linear plot of t/q_t vs t shows the applicability of the pseudo-second-order kinetic model (Periyasamy et al., 2018).

The rate constant (k_{ad}) and r values of the pseudo-first-order and q_e, k, h and r values of the pseudo-second-order kinetic model of Zr@AlgKN composite beads toward NO_3^- and PO_4^{3-} adsorption are listed in Tables 3b and 3c respectively. The q_e value in Table 3b was slightly decreased with increase in temperature during NO_3^- sorption whereas for PO_4^{3-} it was slightly increased with increase in temperature which is shown in Table 3c. Moreover, the higher r value and lower sd value for the pseudo-second-order model than the pseudo-first-order indicates the suitability of the pseudo-second-order kinetic model towards NO_3^- and PO_4^{3-} adsorption.

The particle diffusion and intraparticle diffusion kinetic models were used to investigate the solute transfer during solid-liquid sorption process. The linear plots of ln ($1 - C_t/C_e$) vs t and q_t vs. $t^{0.5}$ denote the suitability of the particle diffusion and intraparticle diffusion kinetic models respectively (Viswanathan et al., 2019). In addition, the values of k_p, k_i and r at 303, 313 and 323 K of both models toward NO_3^- and PO_4^{3-} adsorption are presented in Tables 3b and 3c respectively. It was concluded that the higher r value and lower sd values of the intraparticle diffusion kinetic model declares it suitability for NO_3^- and PO_4^{3-} adsorption compared to particle diffusion kinetic model.

3.10. Exploration of adsorption mechanism

The electrostatic interaction, ion exchange and surface complexation were formed during the adsorption of NO_3^- and PO_4^{3-} by in situ and hydro supported Zr@AlgKN composite beads which are illustrated in Fig. 7. According to Pearson's Hard Soft Acid Base (HSAB) concept, the metal ions with higher positive charge are act as Lewis acid which has an affinity to strongly bind the hard bases such as NO_3^- and PO_4^{3-}. The mobility of NO_3^- and PO_4^{3-} in solution would be the fast towards the protonated Zr—O—OH_2^+, Al—OH_4^+ and Si—OH_5^+ in order to form the electrostatic bond (Lu et al., 2014; Sowmya and Meenakshi, 2014). This electrostatic adsorption was further explained by pH study (cf. Section 3.4). PO_4^{3-} could exist in a multivalent form in water. The dihydrogen phosphate ($H_2PO_4^-$) forms complexation with the protonated Zr—O—OH_2^+, Al—OH_4^+ and Si—OH_5^+ (Fang et al., 2015). Further, the interstitial OH^- ions of kaolin clay may get exchanged for both NO_3^- and PO_4^{3-} by ion-exchange mechanism (Li et al., 2016).

Table 3a Kinetic models, equations and their liner plots.

Kinetic models	Kinetic equation	Linear plot
(i) Reaction-based		
Pseudo-first-order	$\log(q_e - q_t) = \log q_e - \frac{k_{ad}}{2.303} t$	log ($q_e - q_t$) vs t
Pseudo-second-order	$\frac{t}{q_t} = \frac{1}{h} + \frac{t}{q_e}$	t/q_t vs t
(ii) Diffusion-based		
Particle diffusion	$\ln\left(1 - \frac{C_t}{C_e}\right) = -k_p t$	ln ($1 - C_t/C_e$) vs t
Intraparticle diffusion	$q_t = k_i t^{1/2}$	q_t vs $t^{1/2}$

Table 3b Kinetic studies of the hydro supported Zr@AlgKN composite beads for NO_3^- adsorption.

Kinetic models	Parameters	303 K				313 K				323 K			
		80 mg/L	100 mg/L	120 mg/L	140 mg/L	80 mg/L	100 mg/L	120 mg/L	140 mg/L	80 mg/L	100 mg/L	120 mg/L	140 mg/L
Pseudo-first-order	k_{ad} (min^{-1})	0.020	0.023	0.021	0.019	0.023	0.035	0.039	0.027	0.031	0.038	0.033	0.037
	r	0.946	0.945	0.948	0.949	0.950	0.955	0.957	0.959	0.955	0.960	0.962	0963
	sd	0.516	0.524	0.525	0.527	0.511	0.526	0.529	0.561	0.509	0.524	0.558	0.563
Pseudo-second-order	q_e (mg/g)	21.462	31.264	31.269	31.271	21.405	31.259	31.263	31.266	21.389	31.220	31.255	31.261
	k (g/mg min)	0.009	0.017	0.014	0.025	0.008	0.021	0.020	0.012	0.010	0.029	0.030	0.034
	h (mg/g min)	16.234	23.625	23.627	23.630	16.230	23.623	23.625	23.629	16.227	23.621	23.622	23.625
	r	0.995	0.997	0.996	0.999	0.992	0.995	0.996	0.997	0.999	0.997	0.995	0.998
	sd	0.241	0.233	0.230	0.229	0.239	0.235	0.232	0.231	0.237	0.236	0.238	0.240
Particle diffusion	k_p (min^{-1})	0.043	0.087	0.093	0.097	0.067	0.099	0.105	0.107	0.109	0.113	0.115	0.0119
	r	0.942	0.940	0.939	0.941	0.943	0.942	0.940	0.944	0.948	0.949	0.951	0.950
	sd	0.396	0.398	0.399	0.397	0.402	0.415	0.414	0.416	0.416	0.419	0.423	0.417
Intra particle diffusion	k_i (mg/g $min^{0.5}$)	1.023	1.085	1.095	1.099	1.046	1.134	1.128	1.130	1.077	1.154	1.149	1.152
	r	0.985	0.986	0.987	0.990	0.991	0.992	0.988	0.986	0.990	0.994	0.993	0.997
	sd	0.104	0.103	0.106	0.108	0.111	0.113	0.116	0.117	0.120	0.115	0.118	0.121

Table 3c Kinetic studies of the hydro supported Zr@AlgKN composite beads for PO_4^{3-} adsorption.

Kinetic models	Parameters	303 K				313 K				323 K			
		80 mg/L	100 mg/L	120 mg/L	140 mg/L	80 mg/L	100 mg/L	120 mg/L	140 mg/L	80 mg/L	100 mg/L	120 mg/L	140 mg/L
Pseudo-first-order	k_{ad} (min^{-1})	0.034	0.037	0.035	0.027	0.031	0.049	0.053	0.057	0.044	0.043	0.046	0.041
	r	0.966	0.965	0.963	0.969	0.973	0.970	0.972	0.977	0.978	0.986	0.983	0.984
	sd	0.346	0.382	0.386	0.389	0.345	0.376	0.380	0.384	0.343	0.378	0.387	0.392
Pseudo-second-order	q_e (mg/g)	26.032	37.246	37.249	37.252	26.037	37.278	37.284	37.291	26.041	37.290	37.295	37.299
	k (g/mg min)	0.011	0.020	0.028	0.033	0.006	0.025	0.031	0.033	0.015	0.038	0.036	0.031
	h (mg/g min)	19.235	27.135	27.137	27.139	19.236	27.140	27.142	27.144	19.239	27.143	27.146	27.150
	r	0.996	0.998	0.997	0.999	0.993	0.997	0.998	0.999	1.000	0.999	0.997	0.996
	sd	0.154	0.179	0.181	0.177	0.159	0.180	0.178	0.182	0.160	0.175	0.183	0.186
Particle diffusion	k_p (min^{-1})	0.104	0.125	0.128	0.122	0.149	0.167	0.173	0.177	0.159	0.183	0.195	0.199
	r	0.953	0.955	0.952	0.957	0.960	0.954	0.959	0.963	0.961	0.960	0.962	0.965
	sd	0.456	0.469	0.471	0.470	0.459	0.473	0.476	0.478	0.457	0.482	0.485	0.488
Intra particle diffusion	k_i (mg/g $min^{0.5}$)	1.246	1.574	1.678	1.735	1.439	1.628	1.682	1.699	1.538	1.707	1.714	1.735
	r	0.994	0.996	0.995	0.997	0.995	0.994	0.996	0.999	0.998	0.996	0.999	0.995
	sd	0.276	0.293	0.295	0.294	0.277	0.299	0.301	0.302	0.280	0.306	0.309	0.311

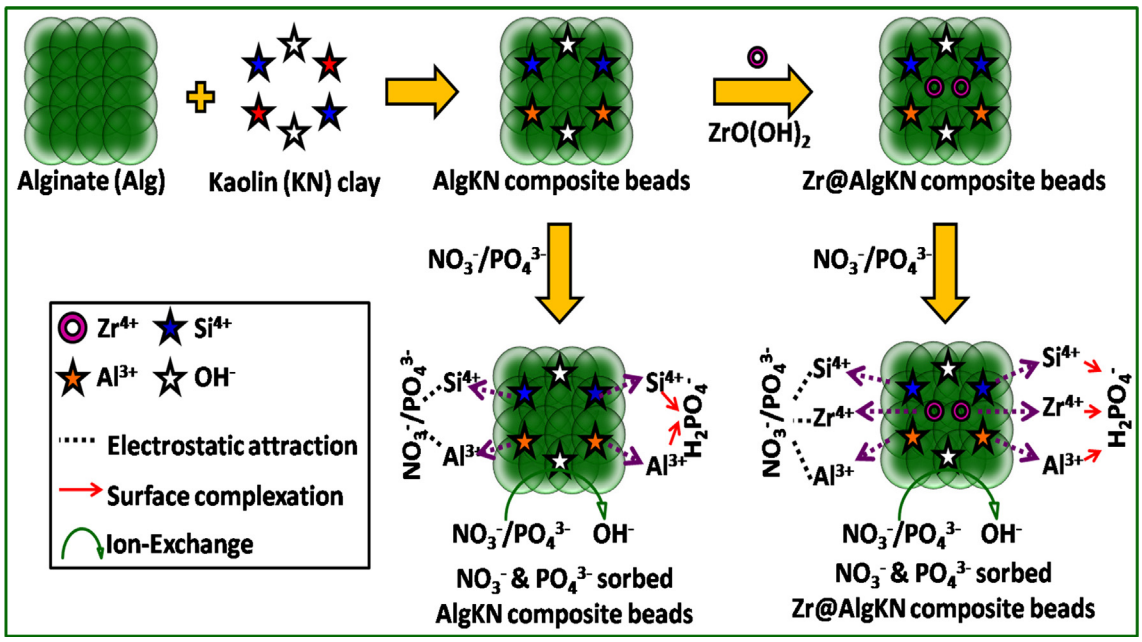

Fig. 7 The possible adsorption mechanism of NO_3^- and PO_4^{3-} using in situ and hydro assisted Zr@AlgKN composite beads.

3.11. Field study of Zr@AlgKN composite beads

The quality parameters of the collected field water samples were investigated using in situ and hydro assisted Zr@AlgKN composite beads and the results are presented in Table 4a. The initial NO_3^- and PO_4^{3-} concentration of the field water sample was found to be 28.16 and 37.42 mg/L respectively. However, the final concentration of NO_3^- and PO_4^{3-} after the treatment was found to be nil. In addition, Cl^- content, total dissolved solids and total hardness of the collected field water was also controlled by the prepared Zr@AlgKN composite beads which ensure its applicability at field conditions.

3.12. Adsorption capacity comparison

The adsorption capacity of the prepared Zr@AlgKN composite beads (Hydro) was compared with the other adsorbents in the market and the comparison is shown in Table 4b. The prepared Zr@AlgKN composite beads possess the appreciable adsorption capacity toward NO_3^- and PO_4^{3-} removal. Although, most of the other adsorbents possess the good adsorption capacity, the powder nature of them leads to attain the pressure drops during filtration which may limit their field applications. However, the prepared Zr@AlgKN composite beads overcome such technological bottle-neck. In addition, Zr@AlgKN composite beads can be easily separated after its usage which designates its applicability at industry level.

3.13. Regeneration study of Zr@AlgKN composite beads

To regenerate the metal ions surrounded adsorbent, a NaOH eluent was used (Wang et al., 2017). Once, the sorption process over, the NO_3^- and PO_4^{3-} sorbed Zr@AlgKN composite beads were completely soaked in 50 mL of 0.1 N NaOH for 1 h followed by filtered, dried at 80 °C and reused for the adsorption again. The same procedure was repeated for six times and their removal efficiency toward NO_3^- and PO_4^{3-} was illustrated in Fig. S3. The increasing cycles of NaOH added decreases the removal percentage. This may governed by the competing effect of basic OH^- ions which occupies the active sites of Zr@AlgKN composite beads surface instead of both NO_3^- and PO_4^{3-}. It was also concluded that there is a significant loss in the NO_3^- and PO_4^{3-} removal percentage was observed after 3 and 4 cycles for in situ and hydro assisted Zr@AlgKN composite beads. Hence, Zr@AlgKN composite beads can be reused as the efficient recyclable adsorbent up to 3 and 3 cycles for water treatment which reveals its cost effective nature.

Table 4a Field test results of Zr@AlgKN composite beads.

Water quality parameters	Before treatment	After treatment	
		Zr@AlgKN (Hydro)	Zr@AlgKN (In situ)
Initial NO_3^- concentration (mg/L)	28.16	Nil	Nil
Initial PO_4^{3-} concentration (mg/L)	37.42	Nil	Nil
pH	5.97	6.63	6.51
Cl^- (mg/L)	328	197	204
Total hardness (mg/L)	539	367	391
Total dissolved solids (mg/L)	454	186	193

Table 4b Evaluation of nitrate and phosphate sorption capacities of the prepared adsorbents in this study with other reported adsorbents.

S. No	Name of the adsorbent	Nitrate			Phosphate			Refs.
		Sorption capacity (mg/g)	Best fit isotherm	Temp. (K)	Sorption capacity (mg/g)	Best fit isotherm	Temp. (K)	
1	Zr@AlgKN composite beads (Hydro)	31.24	Langmuir	303	37.18	Freundlich	303	Present study
2	Modified cellulose from corn stalks	13.60	Langmuir	298	22.88	Langmuir	298	(Fan and Zhang, 2018)
3	Activated carbon prepared from prosopis juliflora	10.99	Langmuir	308	17.33	Langmuir	308	(Manjunath and Kumar, 2018)
4	Fe(0) supported activated carbon	4.60	Langmuir	298	1.75	Langmuir	298	(Khalil et al., 2017)
5	Poly(styrene divinylbenzene)	–	–	–	12.20	Langmuir	303	(Pan et al., 2009)
6	Carbon silica nano composite	11.34	–	–	–	–	–	(Muthu et al., 2017)
7	Zr/quaternary ammonium powder with polyvinylidene fluoride	9.66	–	298	15.58	–	298	(Gao et al., 2019)
8	Bentonite modified with La(III)	–	–	–	14.00	Langmuir	298	(Kuroki et al., 2014)
9	Cu and Mg impregnated alumina	8.00	Freundlich	–	–	–	–	(Jain et al., 2015)
10	Granular chitosan Fe^{3+} complex	8.35	Langmuir & Freundlich	298	–	–	–	(Hu et al., 2015)
11	Biomass	11.20	Langmuir	298	30.20	Langmuir	298	(Kilpimaa et al., 2015)
12	Chitosan saturated with copper (II)	–	–	–	28.86	Langmuir	298	(Dai et al., 2011)

4. Conclusions

The hydro assisted Zr@AlgKN composite beads exhibited an enhanced SC toward NO_3^- and PO_4^{3-} compared to other adsorbents prepared by in situ precipitation method. The solution pH was predominantly affects NO_3^- and PO_4^{3-} sorption and during the protonation of Zr@AlgKN composite beads surface the electrostatic attraction was formed with both NO_3^- and PO_4^{3-}. The serious competence of SO_4^{2-} for NO_3^- and PO_4^{3-} was governed in natural water. FTIR, XRD, SEM, EDAX and BET studies of the adsorbents were studied in detail. The experimental data was fitted with Langmuir and Freundlich isotherms for NO_3^- and PO_4^{3-} adsorption respectively. The order of the NO_3^- and PO_4^{3-} adsorption follows pseudo-second order kinetics and as well as intraparticle diffusion model. The negative ΔH° values of Zr@AlgKN composite beads (Hydro) denote the exothermic nature of NO_3^- adsorption while the positive ΔH° value indicates the endothermic nature of the PO_4^{3-} adsorption. The electrostatic adsorption, surface complexation, and ion-exchange mechanism were involved during NO_3^- and PO_4^{3-} adsorption. The reuse recovery was achieved upto three and four extraction cycles for in situ and hydro assisted Zr@AlgKN composite beads. Moreover, the prepared Zr@AlgKN composite beads were controls the other water quality parameters in addition to NO_3^- and PO_4^{3-} in the collected field water sample which facilitates its applicability at field conditions.

Acknowledgements

The authors were gratefully acknowledging University Grants Commission (F. No. 43-179/2014(SR)), New Delhi, India, for providing financial support to carry out this research work. The first author (I. Aswin Kumar) is sincerely thanks the Council of Scientific and Industrial Research (CSIR), New Delhi, India for awarding Senior Research Fellowship.

Appendix A. Supplementary material

Supplementary data to this article can be found online at https://doi.org/10.1016/j.arabjc.2019.06.006.

References

Adebowale, K.O., Unuabonah, I.E., Olu-Owolabi, B.I., 2006. The effect of some operating variables on the adsorption of lead and cadmium ions on kaolinite clay. J. Hazard. Mater. 134, 130–139.

APHA, 2005. Standard methods for the examination of water and wastewater. American Public Health Association, Washington, DC.

Ahmed, S., Guo, Y., Huang, R., Li, D., Tang, P., Feng, Y., 2017. Hexamethylene tetramine-assisted hydrothermal synthesis of porous magnesium oxide for high-efficiency removal of phosphate in aqueous solution. J. Environ. Chem. Eng. 5, 4649–4655.

Aswin Kumar, I., Viswanathan, N., 2017a. Development of multivalent metal ions imprinted chitosan biocomposites for phosphate sorption. Int. J. Biol. Macromol. 104, 1539–1547.

Aswin Kumar, I., Viswanathan, N., 2017b. Fabrication of metal ions cross-linked alginate assisted biocomposite beads for selective phosphate removal. J. Environ. Chem. Eng. 5, 1438–1446.

Aswin Kumar, I., Viswanathan, N., 2018a. Hydrothermal fabrication of zirconium oxyhydroxide capped chitosan/kaolin framework for highly selective nitrate and phosphate retention. Ind. Eng. Chem. Res. 57 (43), 14470–14481.

Aswin Kumar, I., Viswanathan, N., 2018b. Development and reuse of amine-grafted chitosan hybrid beads in the retention of nitrate and phosphate. J. Chem. Eng. Data 63, 147–158.

Aswin Kumar, I., Viswanathan, N., 2018c. Preparation and testing of a tetra-amine copper(ii) chitosan bead system for enhanced phosphate remediation. Carbohydr. Polym. 183, 173–182.

Aswin Kumar, I., Viswanathan, N., 2018d. A facile synthesis of magnetic particles sprayed gelatin embedded hydrotalcite composite for effective phosphate sorption. J. Environ. Chem. Eng. 6, 208–217.

Aswin Kumar, I., Jeyaprabha, C., Meenakshi, S., Viswanathan, N., 2019. Hydrothermal encapsulation of lanthanum oxide derived *Aegle marmelos* admixed chitosan bead system for nitrate and phosphate retention. Int. J. Biol. Macromol. 130, 527–535.

Bhatnagar, A., Ji, M., Choi, Y.-H., Jung, W., Lee, S.-H., Kim, S.-J., Lee, G., Suk, H., Kim, H.-S., Min, B., Kim, S.-H., Jeon, B.-H., Kang, J.-W., 2008. Removal of nitrate from water by adsorption onto zinc chloride treated activated carbon. Sep. Sci. Technol. 43, 886–907.

Bhatnagar, A., Sillanpaa, M., 2011. A review of emerging adsorbents for nitrate removal from water. Chem. Eng. J. 168, 493–504.

Cui, H., Li, Q., Gao, S., Shang, J.K., 2012. Strong adsorption of arsenic species by amorphous zirconium oxide nanoparticles. J. Ind. Eng. Chem. 18, 1418–1427.

Dai, J., Yang, H., Yan, H., Shangguan, Y., Zheng, Q., Cheng, R., 2011. Phosphate adsorption from aqueous solutions by disused adsorbents: chitosan hydrogel beads after the removal of copper (II). Chem. Eng. J. 166, 970–977.

Dubinin, M.M., Zaverina, E.D., Radushkevich, L.V., 1947. Sorption and structure of active carbons. J. Phys. Chem. 21, 1351–1362.

Fardjaoui, N.E., El Berrichi, F.Z., Ayari, F., 2017. Kaolin-issued zeolite A as efficient adsorbent for bezanyl yellow and nylomine green anionic dyes. Micropor. Mesopor. Mater. 243, 91–101.

Fan, C., Zhang, Y., 2018. Adsorption isotherms, kinetics and thermodynamics of nitrate and phosphate in binary systems on a novel adsorbent derived from corn stalks. J. Geochem. Explor. 188, 95–100.

Fang, L., Huang, L., Holm, P.E., Yang, X., Hansen, H.C.B., Wang, D., 2015. Facile upscaled synthesis of layered iron oxide nanosheets and their application in phosphate removal. J. Mater. Chem. A 3, 7505–7512.

Farzana, M.H., Meenakshi, S., 2015. Photocatalytic aptitude of titanium dioxide impregnated chitosan beads for the reduction of Cr(VI). Int. J. Biol. Macromol. 72, 1265–1271.

Fewtrell, L., 2004. Drinking-water nitrate, methemoglobinemia, and global burden of disease: a discussion. Environ. Health Perspect. 112, 1371–1374.

Freundlich, H.M.F., 1906. Over the adsorption in solution. Zh. Fiz. Khim. 57, 385–470.

Gao, Q., Wang, C.Z., Liu, S., Hanigan, D., Liu, S.T., Zhao, H.Z., 2019. Ultrafiltration membrane micro reactor (MMR) for simultaneous removal of nitrate and phosphate from water. Chem. Eng. J. 355, 238–246.

Georges-Ivo, E.E., 2005. Fourier transform infrared spectrophotometry and X-ray powder diffractometry as complementary techniques in characterizing clay size fraction of kaolin. J. Appl. Sci. Environ. Manage. 9, 43–48.

Guo, C.H., Stabnikov, V., Ivanov, V., 2010. The removal of nitrogen and phosphorus from reject water of municipal wastewater treatment plant using ferric and nitrate bioreductions. Bioresour. Technol. 101, 3992–3999.

Hu, Q., Chen, N., Feng, C., Hu, W., 2015. Nitrate adsorption from aqueous solution using granular chitosan-Fe^{3+} complex. Appl. Surf. Sci. 347, 1–9.

Jain, S., Bansiwal, A., Biniwale, R.B., Milmille, S., Das, S., Tiwari, S., Antony, P.S., 2015. Enhancing adsorption of nitrate using metal impregnated alumina. J. Environ. Chem. Eng. 3, 2342–2349.

Karimi, M., Shojaei, A., Nematollahzadeh, A., Abdekhodaie, M.J., 2012. Column study of Cr (VI) adsorption onto modified silica–polyacrylamide microspheres composite. Chem. Eng. J. 210, 280–288.

Khalil, A.M.E., Eljamal, O., Amen, T.W.M., Sugihara, Y., Matsunaga, N., 2017. Optimized nano-scale zero-valent iron supported on treated activated carbon for enhanced nitrate and phosphate removal from water. Chem. Eng. J. 309, 349–365.

Kilpimaa, S., Runtti, H., Kangas, T., Lassi, U., Kuokkanen, T., 2015. Physical activation of carbon residue from biomass gasification: novel sorbent for the removal of phosphates and nitrates from aqueous solution. J. Ind. Eng. Chem. 21, 1354–1364.

Kuroki, V., Bosco, G.E., Fadini, P.S., Mozeto, A.A., Cestari, A.R., Carvalho, W.A., 2014. Use of La(III)-modified bentonite for effective phosphate removal from aqueous media. J. Hazard. Mater. 274, 124–131.

Kyu-Hong, A., Kyung-Guen, S., Eulsaeng, C., Jinwoo, C., Hojoon, Y., Seockheon, L., Jaeyoung, M., 2003. Enhanced biological phosphorus and nitrogen removal using a sequencing anoxic/anaerobic membrane bioreactor (SAM) process. Desalination 15, 345–352.

Langmuir, I., 1916. The constitution and fundamental properties of solids and liquids. J. Am. Chem. Soc. 38, 2221–2295.

Li, R., Wang, J.J., Zhou, B., Awasthi, M.K., Ali, A., Zhang, Z., Gaston, L.A., Lahori, A.H., Mahar, A., 2016. Enhancing phosphate adsorption by Mg/Al layered double hydroxide functionalized biochar with different Mg/Al ratios. Sci. Total Environ. 559, 121–129.

Lopez-Ramon, M.V., Stoeckli, F., Moreno-Castilla, C., Carrasco-Marin, F., 1999. On the characterization of the acidic and basic surface sites on carbons by various techniques. Carbon 37, 1215–1221.

Lu, J., Liu, H., Zhao, X., Jefferson, W., Cheng, F., Qu, J., 2014. Phosphate removal from water using freshly formed Fe-Mn binary oxide: adsorption behaviors and mechanisms. Colloids Surf., A 455, 11–18.

Manjunath, S.V., Kumar, M., 2018. Evaluation of single and multi-component adsorption of metronidazole, phosphate and nitrate on activated carbon from prosopis juliflora. Chem. Eng. J. 346, 525–534.

Meinhold, J., Arnold, E., Isaacs, S., 1999. Effect of nitrite on anoxic phosphate uptake in biological phosphorus removal activated sludge. Water Res. 33, 1871–1883.

Mekhemer, G.A.H., 1998. Characterization of phosphated zirconia by XRD, Raman and IR spectroscopy. Colloids Surf., A 141, 227–235.

Muthu, M., Ramachandran, D., Hasan, N., Jeevanandam, M., Gopal, J., Chun, S.C., 2017. Unprecedented nitrate adsorption efficiency of carbon-silicon nanocomposites prepared from bamboo leaves. Mater. Chem. Phys. 189, 12–21.

Niwas, R., Gupta, U., Khan, A.A., Varshney, K.G., 2000. The adsorption of phosphamidon on the surface of styrene supported zirconium (IV) tungstophosphate: A thermodynamic study. Colloids Surf., A 164, 115–119.

Njoya, A., Nkoumbou, C., Grosbois, C., Njopwouo, D., Njoya, D., Courtin-Nomade, A., 2006. Genesis of mayouom kaolin deposit (Western Cameroon). Appl. Clay Sci. 32, 125–140.

Pahlavanzadeh, H., Katal, R., Mohammadi, H., 2012. Synthesize of polypyrrole nanocomposite and its application for nitrate removal from aqueous solution. J. Ind. Eng. Chem. 18, 948–956.

Pan, B., Wu, J., Pan, B., Lv, L., Zhang, W., Xiao, L., Wang, X., Tao, X., Zheng, S., 2009. Development of polymer-based nanosized hydrated ferric oxides (HFOs) for enhanced phosphate removal from waste effluents. Water Res. 43, 4421–4429.

Pandi, K., Viswanathan, N., 2014. Synthesis of alginate bioencapsulated nano-hydroxyapapatite composite for selective fluoride sorption. Carbohydr. Polym. 112, 662–667.

Pandi, K., Viswanathan, N., 2015. A novel metal coordination enabled in carboxylated alginic acid for effective fluoride removal. Carbohydr. Polym. 118, 242–249.

Periyasamy, S., Gopalakannan, V., Viswanathan, N., 2018. Hydrothermal assisted magnetic nanohydroxyapatite encapsulated alginate beads for efficient Cr (VI) uptake from water. J. Environ. Chem. Eng. 6, 1443–1454.

Saad, R., Belkacemi, K., Hamoudi, S., 2007. Adsorption of phosphate and nitrate anions on ammonium-functionalized MCM-48: effects of experimental conditions. J. Colloid Interface Sci. 311, 375–381.

Sowmya, A., Meenakshi, S., 2014. Effective removal of nitrate and phosphate anions from aqueous solutions using functionalized chitosan beads. Desalin. Water Treat. 52, 2583–2593.

Thagira Banu, H., Karthikeyan, P., Meenakshi, S., 2018. Lanthanum (III) encapsulated chitosan-montmorillonite composite for the adsorptive removal of phosphate ions from aqueous solution. Int. J. Biol. Macromol. 112, 284–293.

Viswanathan, N., Aswin Kumar, I., Meenakshi, S., 2019. Development of chitosan encapsulated tricalcium phosphate biocomposite for fluoride retention. Int. J. Biol. Macromol. 133, 811–816.

Wang, S., Nan, Z., Li, Y., Zhao, Z., 2009. The chemical bonding of copper ions on kaolin from suzhou, China. Desalination 249, 991–995.

Wang, X., Zhang, G., Lan, H., Liu, R., Liu, H., Qu, J., 2017. Preparation of hollow Fe-Al binary metal oxyhydroxide for efficient aqueous fluoride removal. Colloids Surf. A 520, 580–589.

Wu, C.-H., 2007. Adsorption of reactive dye onto carbon nanotubes: equilibrium, kinetics and thermodynamics. J. Hazard. Mater. 144, 93–100.

Xing, X., Bao-Yu, G., Qin-Yan, Y., Qian-Qian, Z., 2010. Preparation of agricultural by-product based anion exchanger and its utilization for nitrate and phosphate removal. Bioresour. Technol. 101, 8558–8564.

Zhao, X.H., Li, Q., Ma, X.M., Xiong, Z., Quan, F., Xia, Y.Z., 2015. Alginate fibers embedded with silver nanoparticles as efficient catalysts for reduction of 4-nitrophenol. RSC Adv. 5, 49534–49540.